THE UNUSUAL RADIO GALAXY 3C 288

ALAN H. BRIDLE AND EDWARD B. FOMALONT
National Radio Astronomy Observatory,[a] Edgemont Road, Charlottesville, Virginia 22903-2475

GENE G. BYRD
Department of Physics and Astronomy, University of Alabama, Tuscaloosa, Alabama 35487-1921

MAURI J. VALTONEN
Turku University Observatory, Itäinen Pitkäkatu 1, 20520 Turku 52, Finland
Received 27 September 1988; revised 28 November 1988

ABSTRACT

The VLA has been used to image the radio galaxy 3C 288 at 1.5, 4.9, and 15 GHz (20, 6, and 2 cm), revealing several new features of this unusually powerful edge-darkened radio source. These features include a jet and counterjet near the radio core, and faint "wings" of emission connected to the elongated lobes. There are large spectral gradients across the lobes, and the jet and counterjet have different spectra between 4.9 and 15 GHz. The south lobe, which is fed by the brighter jet, is more strongly polarized than the north lobe. Both lobes depolarize significantly between 4.9 and 1.5 GHz; this effect is smallest in the outer parts of the south lobe, and increases toward the center of the source and toward the outer parts of the north lobe. Although the edge darkening of the radio structure, and its spectral-index distribution, are reminiscent of a (distorted) radio "trail," no other properties of 3C 288 suggest that it belongs to this morphological class. The radio luminosity would be unusually high for a trail source and the host galaxy is probably the dominant member of a distant cluster. There are weak features that may be incipient "hotspots" as in powerful double sources. The jet/counterjet structure lacks the prominent C symmetry of a trail source, but has asymmetries that are all consistent with mildly relativistic outflows that have recently restarted. The larger-scale structure of 3C 288 may be an example of a disturbed secondary-flow pattern, rather than a structure shaped primarily by bending of the primary flow as a result of the motion of its parent galaxy.

I. INTRODUCTION

The radio source 3C 288 is identified with a D4 elliptical galaxy with $m_V = 18.3$ (Goodson *et al.* 1979) and $z = 0.246$ (Smith and Spinrad 1980). Its luminosity distance, assuming $H_0 = 100h$ km s^{-1} Mpc^{-1} and $q_0 = 0.5$, is $778h^{-1}$ Mpc. There are fainter galaxies in the field which are presumed to be a cluster, of which 3C 288 is the dominant member (Wyndham 1966). Its monochromatic power at 1.5 GHz is $2.5h^{-2}\times10^{26}$ W Hz^{-1} and its integrated spectral index $\alpha_5^{0.75}$ between 0.75 and 5 GHz is 0.97 (Laing and Peacock 1980, $S(\nu) \propto \nu^{-\alpha}$). Most steep-spectrum 3C radio galaxies that have radio powers similar to that of 3C 288 are edge-brightened "classical doubles," e.g., 3C 33.1 ($P_{1.4} = 1.3h^{-2}\times10^{26}$ W Hz^{-1}—van Breugel 1980; Rudnick 1985), and 3C 219 ($P_{1.4} = 2.8h^{-2}\times10^{26}$ W Hz^{-1}—Bridle *et al.* 1986).

A 5 GHz observation at 2″ ($4.9h^{-1}$ kpc) resolution with the Cambridge 5 km telescope (Pooley and Henbest 1974; henceforth referred to as PH) showed that 3C 288 has two broad radio lobes about 20″ ($50h^{-1}$ kpc) wide but only 10″ apart. These data showed that the emission extends much further to the west of the optical identification than to the east. This asymmetry raised the possibility that 3C 288 might be related to the radio "trail," or "head–tail" sources (e.g., Valtonen 1976).

Both the radio power and the optical identification of 3C 288 would be remarkable for a radio trail source, however. The mean integrated power of the sample of 51 "narrow-angle tails" studied by O'Dea and Owen (1985) is $P_{1.4} = 1.0h^{-2}\times10^{24}$ W Hz^{-1}, about two hundred times less than that of 3C 288, and the most luminous trail in their sample has $P_{1.4} = 2.8h^{-2}\times10^{25}$ W Hz^{-1}, about nine times less than that of 3C 288. Furthermore, if the galaxy identified with 3C 288 is truly associated with the cluster, it is the cluster's dominant member by about 2 mag. Dominant galaxies are generally at or near the dynamical centers of their clusters (Quintana and Lawrie 1982). This should inhibit the formation of narrow-angle trails by the canonical ram-pressure jet-bending mechanism (e.g., Begelman *et al.* 1979), and indeed no well-defined narrow-angle trail source has been found to be associated with a dominant cluster member.

Dominant cluster members can produce asymmetric "wide-angle-tail" (WAT) radio structures (e.g., Burns 1986, and references therein), despite their presumed low peculiar velocities, but the wide-lobed radio structure of 3C 288 as determined by PH is not a clear example of WAT morphology. The source's luminosity and size would also be an unusual combination for a WAT. Most of the prototypical WATs are notably less luminous than 3C 288, with powers in the range $2h^{-2}\times10^{24} < P_{1.4} < 2h^{-2}\times10^{25}$ W Hz^{-1}. The more powerful WATs are also typically $> 200h^{-1}$ kpc in extent (Burns 1986), and so are larger than 3C 288 (at least in projection).

The structure of 3C 288 is more asymmetric than those of normal double sources of its size and radio power, yet it cannot be associated convincingly with any of the well-recognized classes of asymmetric radio morphologies. These properties motivated us to reobserve the source with the VLA in an attempt to clarify its relationship to other radio galaxies. We obtained both higher-resolution, and lower-frequency, data than those of PH to see whether 3C 288 has radio jets, hotspots, or steep-spectrum "plumes" that might help us to classify the structure. We also sought to test a "nonstandard" model for 3C 288 based on the ejection of

[a] The NRAO is operated by Associated Universities, Inc., under contract with the National Science Foundation.

 0004-6256/89/030674-12$00.90

supermassive objects from the nucleus of a moving galaxy (Valtonen 1976; Byrd and Valtonen 1980), as this model explicitly predicted the brightness distribution of the source at 5 GHz.

II. OBSERVATIONS

We observed 3C 288 with 23 antennas at 1.465 GHz and 4.885 GHz in a nonstandard configuration during the construction of the VLA, and again at 4.885 GHz and 14.965 GHz in the VLA's standard A configuration. Table I lists the main observational parameters. The flux-density scales of all observations were normalized to that of Baars *et al.* (1977) by observing 3C 286, whose flux density on their scale is 14.51 Jy at 1.465 GHz, 7.41 Jy at 4.885 GHz, and 3.45 Jy at 14.965 GHz. The flux-density normalization is believed to be accurate to $\pm$ 2% at all three frequencies. The phases and the positional reference frame were initially calibrated by interpolation from observations of the unresolved calibrator 1308 + 326. The observations of this source were also used to determine the on-axis instrumental cross-polarization properties. The zero point of the E vector position angles χ was set at each frequency by observations of 3C 286, which was assumed to have $\chi = 33°$.

The images were made, self-calibrated (Schwab 1980), and deconvolved (CLEANed—Högbom 1974; Clark 1980; Steer *et al.* 1984) using the NRAO's AIPS image-processing software. Table II lists the main parameters of the images. The resolution was varied by applying Gaussian tapering functions falling to 30% at the radii listed in the table. The beams used to smooth the final images were circularized during the CLEAN restoration by increasing the minor axes of the elliptical Gaussian "CLEAN beams" fitted to the central responses of the synthesized "dirty" beams.

The shortest (projected) baselines in the data taken during the construction of the VLA correspond to fringe separations of 16′ at 1.5 GHz and 8′.4 at 4.9 GHz. These fringe separations are much larger than the largest angular scale present in 3C 288, which we find to be about 36″. We therefore expect that all the emission is properly represented in the images made from the data taken in the construction configuration. The integrated flux densities in these images are 3.34 Jy at 1.5 GHz, and 0.95 Jy at 4.9 GHz. These are within measurement uncertainties of the flux densities derived from single-dish observations, i.e., 3.41 $\pm$ 0.09 Jy at 1.5 GHz (Bridle *et al.* 1972, adjusted to the Baars *et al.* scale) and 0.98 $\pm$ 0.06 Jy at 5.0 GHz (Laing and Peacock 1980). In contrast, the shortest (projected) baselines in the A configuration data correspond to fringe separations of 20″ at 4.9 GHz and 5″.6 at 15 GHz. Emission features with equivalent Gaussian FWHMs $> 9''$ at 4.9 GHz and $> 2''.5$ at 15 GHz will be attenuated by $> 50\%$ in images made from these data alone. We therefore restrict our use of the A configuration data to high-resolution imaging of the central parts of the source.

III. TOTAL AND POLARIZED EMISSION

a) Total Intensity

Figure 1 displays contours of the total intensity (Stokes *I*) at 1.5 GHz, showing the main structural features of 3C 288 with 1″.6 ($3.9h^{-1}$ kpc) resolution. This image was deconvolved using the AIPS implementation of the smoothness-stabilized CLEAN algorithm developed by Steer *et al.* (1984). As no additional emission was visible on the image made from these data at 2″.9 ($7.1h^{-1}$ kpc) resolution, and the integrated flux density in Fig. 1 agrees with the single-dish flux density, we believe that this image represents most of the 1.5 GHz emission from 3C 288.

A central emission peak is linked by a narrow ridge $\sim 5''$ ($12h^{-1}$ kpc) long to a pair of broad lobes, in agreement with the PH data. The crosses mark the optical positions of the two brightest galaxies in the field; the identification is the galaxy close to the peak of the ridge. Both lobes have low-intensity "wings" that extend for $\sim 15''$ ($36h^{-1}$ kpc) to the northwest and southwest of the structure documented by PH. The largest (projected) dimension of the source now appears to be 36″ ($88h^{-1}$ kpc).

Figure 1 suggests that the wings of the north lobe might form a C-shaped structure with the second galaxy at its apex. However, none of our higher-resolution images suggests that this second galaxy is a radio source. We therefore presume that all the emission is associated with the eastern galaxy.

Figure 2 displays contours of the total intensity at 4.9 GHz with 0″.6 ($1.5h^{-1}$ kpc) resolution. The optical identification is at the peak of the bright central ridge of emission; the cross marks the optical position of the second galaxy. In this image, the central ridge is unresolved transverse to its length, but is resolved into three or more discrete knots along

TABLE I. Observing parameters.

Observing Date	25 Mar 1980	25 Mar 1980	31 Oct 1983	31 Oct 1983
Frequency	1.465 GHz	4.885 GHz	4.885 GHz	14.965 GHz
Integration time	2.7 hrs	3.3 hrs	0.6 hrs	4.0 hrs
HA range	± 4 hrs	± 4 hrs	± 4 hrs	± 4 hrs
Bandwidth	50 MHz	50 MHz	50 MHz	50 MHz
Configuration	constr.	constr.	A	A
Min proj. baseline	43 m	25 m	620 m	735 m
Max proj. baseline	24.6 km	24.6 km	36 km	36 km
Primary HPBW	31 arcmin	9.2 arcmin	9.2 arcmin	3 arcmin

TABLE II. Imaging parameters.

Frequency (GHz)	CLEAN Beam FWHM (″)	Configuration	Taper (kλ)	RMS noise (μJy/beam)	Flux inserted at $u,v = 0$ (Jy)
1.465	2.9	constr.	60	I 240	3.4
1.465	1.6	constr.	none	I 150	3.4
				QU 140	
4.885	1.6	constr., excluding all >120kλ	none	I 150	0.98
				QU 90	
4.885	0.6	constr.	none	IQU 75	0.98
4.885	0.38	A	none	IQU 80	0.98
14.965	0.38	A	325	IQU 170	0.24
14.965	0.2	A	600	IQU 110	0.24
14.965	0.09	A	none	IQU 120	0.24

P.A. ~147°. It resembles a jet/counterjet structure with an embedded core, and this impression is confirmed by our higher-resolution images (Fig. 3). We therefore refer to the resolved features of the central ridge as the jet or counterjet in what follows.

The brightest emission in the south lobe is at its east end, in a ridge ~3″ ($7.2h^{-1}$ kpc) long, oriented approximately north–south. The north end of this ridge turns towards the jet axis but does not clearly connect to the jet itself. Its south end turns along the south edge of the lobe, where it persists as a slightly brightened rim for about 8″ ($20h^{-1}$ kpc). The brightest emission in the north lobe is at its west end. It is a ridge ~4″ ($9.6h^{-1}$ kpc) long, oriented approximately east–west. Its northwest end contains a bright, resolved, knot next to the steepest brightness gradient in the source. Its east end turns towards the jet axis but does not clearly connect to the bright jet/counterjet structure. The north lobe contains a second ridge, also ~4″ long, along its southeast edge. The west end of this ridge is also close to the jet axis, and turns towards it. The pattern of these ridges makes the north lobe as a whole appear slightly center darkened.

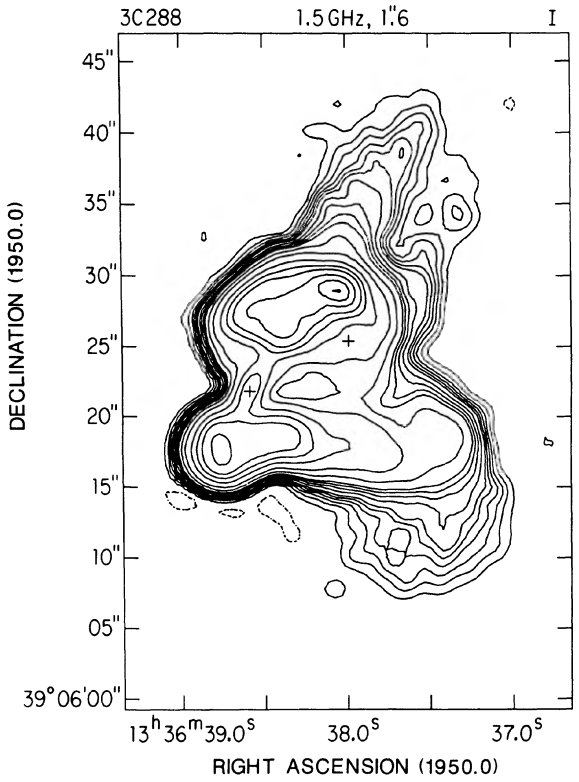

FIG. 1. Total-intensity distribution at 1.5 GHz, from VLA construction configuration data with 1.″6 resolution. Contours are drawn at −1 (dotted), 1, 2, 3, 4, 5, 6, 8, 10, 12, 14, 20, 30, 50, 70, 90, 120, 150, 180, and 210 times 650 μJy per CLEAN beam area. The crosses mark the centers of the two galaxies whose images lie within the radio structure.

Both Fig. 1 and Fig. 2 show that the lobes are smoother than was suggested by the PH data, despite the high angular resolution of Fig. 2, and the presence of the ridges. The outer wings seen in Fig. 1 are heavily resolved in Fig. 2, though faint emission (too close to the rms noise to appear on the contour plot) is present at the locations of both wings.

Figure 3 displays contours of the total intensity around the core source from the A configuration observations at 4.9 GHz with 0.″38 ($920h^{-1}$ pc) resolution and at 14.9 GHz with both 0.″38 and 0.″2 ($460h^{-1}$ pc) resolution. The radio core is the brightest and most compact feature on all three images. Its flux densities, estimated from Fig. 3(a) and from a 15 GHz image at 0.″09 ($220h^{-1}$ pc) resolution, are 9.7 ± 0.3 mJy and 10.6 ± 0.5 mJy at 4.9 and 15 GHz, respectively. Its (epoch 1950.0) position, determined at 15 GHz with respect to the *optical* position of the external phase calibrator 1308 + 326, is $13^h36^m38^s.588$, +39°06′21.″76, with errors of ± 0.″2 in each coordinate. This coincides with the optical position of the nucleus of 3C 288 as measured by Goodson *et al.* (1979), which is $13^h36^m38^s.59$, +39°06′21.″8, with errors of ± 0.″4 in each coordinate.

All the other knots in the central region of the source are resolved with the beam sizes used in Fig. 3. These knots are clearly part of an asymmetric jet/counterjet structure in which the brighter jet is south of the core. This jet is resolved transverse to its length at 15 GHz, the deconvolved FWHM of the knots 0.″8 and 1.″5 ($1.9h^{-1}$ and $3.6h^{-1}$ kpc) from the core being 0.″12 ($290h^{-1}$ pc) and 0.″17 ($410h^{-1}$ pc), respectively. The counterjet is barely detected at 15 GHz. The two images at 0.″38 resolution (Figs. 3(a) and 3(b)) show that the faintness of the counterjet at 15 GHz is not an artifact of resolution relative to the main jet—the spectral indices $\alpha_{15}^{4.9}$ of the jet and counterjet between 4.9 and 15 GHz at 0.″38 resolution are 0.72 ± 0.04 and 1.30 ± 0.17, respectively.

Table III lists the integrated flux densities and spectral indices of the main features of the source, in each case determined at the lowest resolution at which they could be sepa-

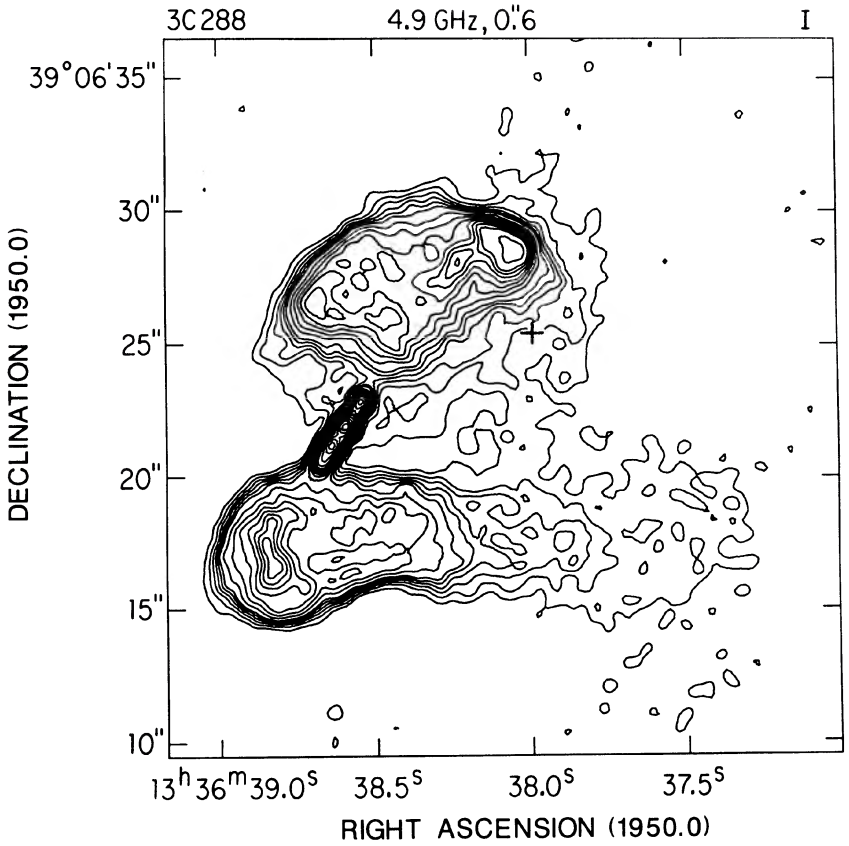

FIG. 2. Total-intensity distribution at 4.9 GHz, from VLA construction configuration data with 0."6 resolution. Contours are drawn at − 1 (dotted), 1, 2, 3, 4, 5, 6, 8, 10, 12, 14, 16, 18, 20, 24, 30, 36, and 50 times 275 μJy per CLEAN beam area. The center of the parent galaxy coincides with the peak of radio emission in the central ridge; the center of the second galaxy is marked by the cross.

rated from other features. To estimate the integrated spectrum of the extended components of the jet and counterjet between 1.5 and 4.9 GHz, we assume the flux density of the core to be 10 mJy at 1.5 GHz, i.e., that it has $\alpha_{4.9}^{1.5} = 0$.

Figure 4 superimposes a gray-scale plot of the distribution of the spectral index $\alpha_{4.9}^{1.5}$ at 1."6 resolution on selected contours from Fig. 1. The 4.9 GHz image at this resolution was also deconvolved using the Steer *et al.* (1984) CLEAN algorithm. The lowest spectral index, $\alpha_{4.9}^{1.5} = 0.6$, occurs at the core and applies to a blend of core and jet emission. The

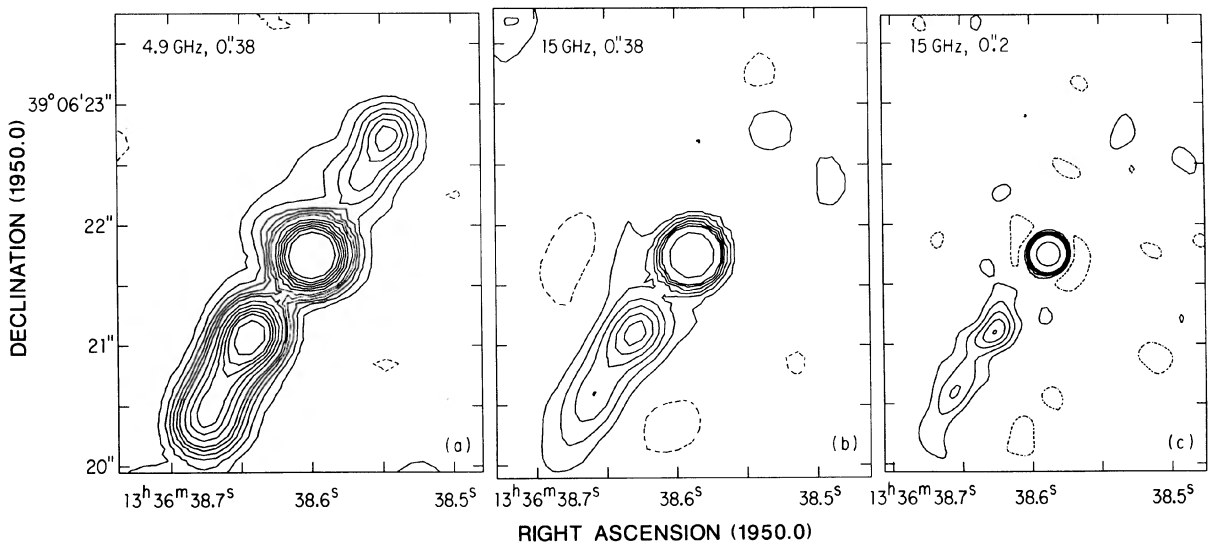

FIG. 3. Total-intensity distributions over the central region of the source at (a) 4.9 GHz with 0."38 resolution, (b) 15 GHz with 0."38 resolution, and (c) 15 GHz with 0."2 resolution, from the VLA A configuration data. Contours in (a) are drawn at − 1 (dotted), 1, 2, 3, 4, 5, 6, 8, 10, 12, 14, 16, and 19.92 times 250 μJy per CLEAN beam area. Contours in (b) are at − 1 (dotted), 1, 2, 3, 4, 5, 6, and 10.78 times 400 μJy per CLEAN beam area, and those in (c) are at − 1 (dotted), 1, 2, 3, 4, 5, and 16.3 times 300 μJy per CLEAN beam area. In each display, the highest contour shows the FWHM of the CLEAN restoring beam.

TABLE III. Flux densities and spectral indices of features in 3C 288.

	1.5 GHz (mJy)	4.9 GHz (mJy)	15 GHz (mJy)	$\alpha_{4.9}^{1.5}$	$\alpha_{15}^{4.9}$
Jet+Counterjet+Core	160 ± 15	70 ± 5		0.69 ± 0.05	
South Jet Knots		15.3 ± 0.7	6.8 ± 0.3		0.72 ± 0.04
North Jet Knots		3.2 ± 0.3	0.75 ± 0.2		1.30 ± 0.17
Core		9.7 ± 0.3	10.6 ± 0.5		
Jet+Counterjet	(150)	60 ± 5		0.76 ± 0.1	
North lobe	1800 ± 50	480 ± 15		1.10 ± 0.03	
South lobe	1400 ± 50	400 ± 15		1.04 ± 0.03	
Total source	3410 ± 90	980 ± 60	240 ± 10	1.04 ± 0.03	1.26 ± 0.05

lowest spectral indices in the lobes are $\alpha_{4.9}^{1.5} = 0.8$, and occur in the ridges at the eastern ends of both lobes. The spectral indices increase to $\alpha_{4.9}^{1.5} = 1.5$ westwards across the lobes, while the diffuse "wings" have steeper spectra, with $\alpha_{4.9}^{1.5} \geqslant 1.7$. Section IV(a) interprets these spectral variations quantitatively.

b) Polarized Emission

Figure 5(a) displays contours of the linearly polarized intensity ($P = \sqrt{Q^2 + U^2}$) at 4.9 GHz with 0.″6 (1.5h^{-1} kpc) resolution. Figure 5(b) displays vectors whose lengths are proportional to the degree of linear polarization $p = P/I$ and whose position angles χ are those of the observed **E** vectors. The estimates of p have been corrected for the bias in the Ricean distribution of P (e.g., Wardle and Kronberg 1974) using the values listed in Table II for the standard deviations of the Gaussian distributions of Q and U. Vectors are plotted every FWHM wherever the signal-to-noise ratio of the polarized intensity is $>4{:}1$.

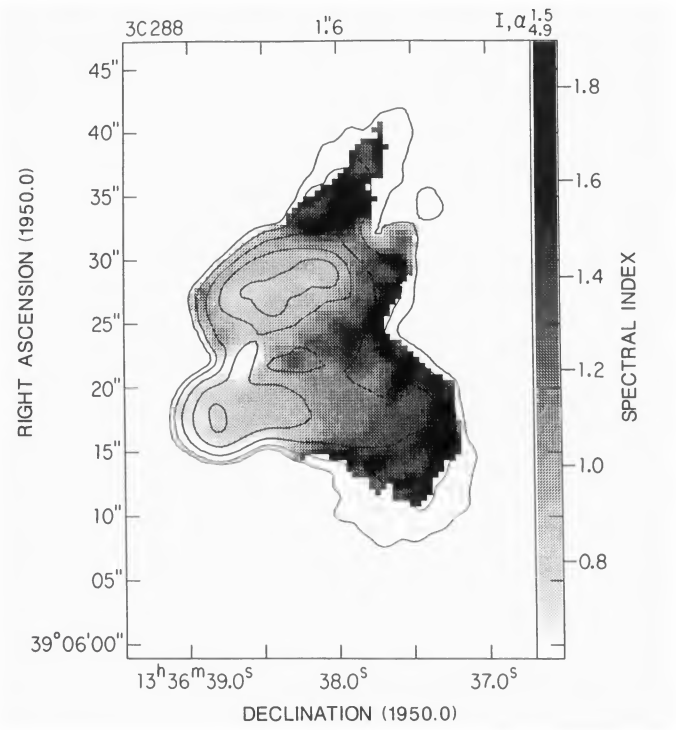

FIG. 4. Distribution of the 1.5–4.9 GHz spectral index $\alpha_{4.9}^{1.5}$ with 1.″6 resolution, shown as a gray scale superimposed on selected contours from Fig. 1. The spectral index is shown only where the signal-to-noise ratio at 1.5 GHz exceeds 6:1 and that at 4.9 GHz exceeds 4:1. The low-level striations in this display are believed to result from imperfections in the CLEAN deconvolution.

Figure 5 shows that the two lobes have strikingly different polarized intensities at 4.9 GHz; the south lobe is much more strongly polarized than the north. At 0.″6 resolution, the degree of linear polarization at 4.9 GHz, $p_{4.9}$, is ~0.1 to 0.2 at the east end of the lobe, and increases to ~0.4 west of the bright ridge. Further west, there is a band across the center of the lobe where $p_{4.9}$ drops to ~0.1, but $p_{4.9}$ increases again to ~0.45 along the south rim of the lobe, and to ~0.55 at its western end. In contrast $p_{4.9} < 0.1$ over most of the north lobe, the exceptions being a region near the western edge of the lobe where it reaches 0.35, and near the knot at the base of the longer wing, where $p_{4.9} \approx 0.15$.

The degree of polarization in the lobes also varies with frequency at fixed resolution. Figure 6 compares the distributions of p and χ over the lobes with 1.″6 resolution at 1.5 and 4.9 GHz. Figure 6(d) confirms the general increase in $p_{4.9}$ from east to west across the south lobe at 4.9 GHz. It also traces the polarized signal further into the diffuse wings, where $p_{4.9} \approx 0.6$ in both lobes at this resolution. In contrast, Fig. 6(b) shows that the 1.5 GHz degree of polarization $p_{1.5}$ is typically 0.005–0.02 at the east end of the south lobe, and rises only to $p_{1.5} = 0.08$ towards its west end. The depolarization $D_{4.9}^{1.5} = p_{1.5}/p_{4.9}$ ranges from 0.04 to 0.12 at the east end of the south lobe, and from 0.1 to 0.25 at the west end. The emission is therefore more depolarized near the center of the galaxy than in the outer parts of the south lobe.

Figure 6(a) shows that no significant polarized emission is detected at 1.5 GHz in the north lobe; $p_{1.5}$ is typically $\leqslant 0.01$ over this lobe. Upper limits to the depolarization $D_{4.9}^{1.5}$ can be given wherever the polarized signal was detected in the north lobe at 4.9 GHz. At a few such places in the outer lobe, $D_{4.9}^{1.5} < 0.1$. There is therefore some evidence that the outer north lobe depolarizes more between 4.9 and 1.5 GHz than does the outer south lobe.

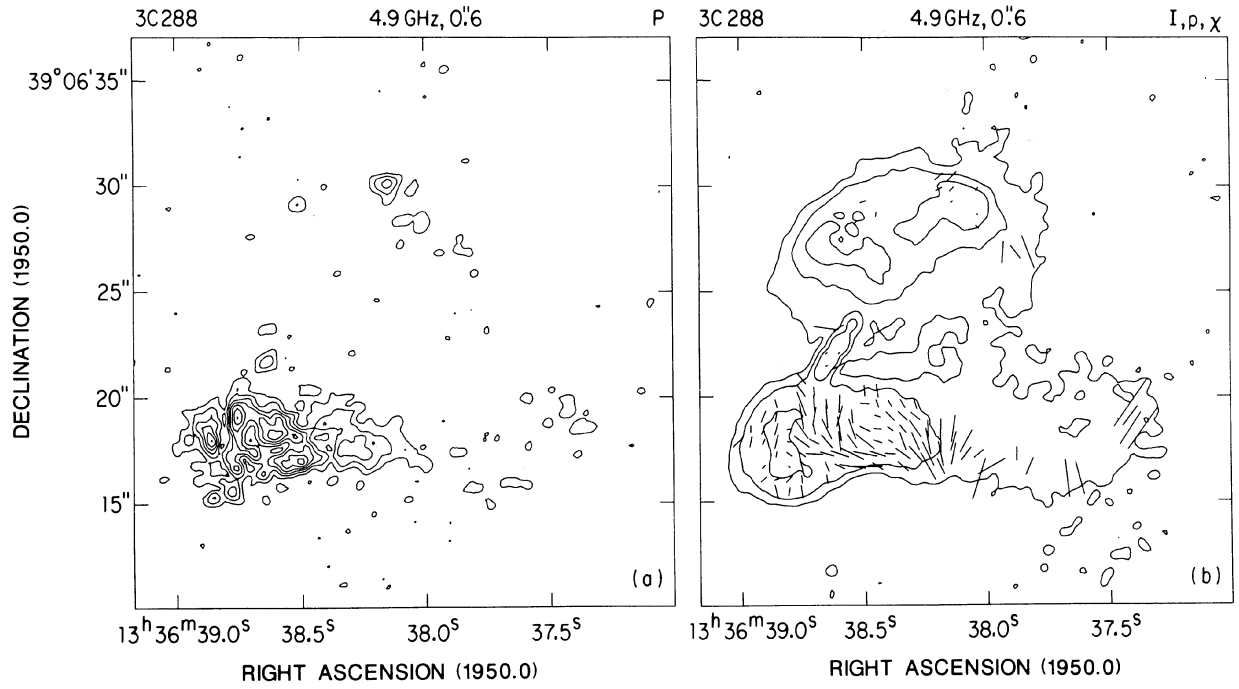

FIG. 5. (a) Distribution of polarized intensity at 4.9 GHz with 0".6 resolution. Contours are drawn at 1, 2, 3, 4, 5, 6, and 7 times 225 μJy per CLEAN beam area. (b) Distribution of the degree of linear polarization $p_{4.9}$ and E vector position angles χ at 4.9 GHz with 0".6 resolution. Contours are chosen to delineate the main features of the total-intensity distribution shown in Fig. 2. The vectors have lengths proportional to $p_{4.9}$ (a vector of length 1" being equivalent to $p_{4.9} = 0.333$). Vectors are drawn at intervals of 0".6, wherever the polarized signal-to-noise ratio is $> 4{:}1$.

The low degrees of polarization at 1.5 GHz, and the lack of a third observing frequency at 1".6 resolution, prevent us from determining the Faraday rotation measure (RM) distribution uniquely, but there is evidence that RM fluctuates over the south lobe. Local values would range from -35 radians m^{-2} to $+20$ radians m^{-2}, *if* the RM is everywhere the minimum consistent with the rotation $\Delta\chi$ observed between 4.9 and 1.5 GHz. This assumption is questionable, however, for this range of RM is close to the maximum that can be measured unambiguously between these frequencies.

To summarize, there is good evidence that the degree of polarization of both lobes decreases significantly with frequency between 1.5 and 4.9 GHz. This is consistent with the unusually short "half depolarization wavelength" ($\lambda_{1/2} = 7$ cm) found for the integrated polarization of 3C 288 (Conway *et al.* 1983; Strom and Conway 1983). There is also evidence for faster depolarization of the north (counterjet) lobe. The available data do not allow us to characterize either the extent or the location of the Faraday screen responsible for these effects. They do, however, suggest that 3C 288 follows the trend, exhibited by other powerful sources, for the brighter radio jet to be on the same side as the lobe with the lesser depolarization (Garrington *et al.* 1988; Laing 1988).

Figure 7 shows the 4.9 GHz polarization data for the central region alone at 0".38 ($920h^{-1}$ pc) resolution. The asymmetry in the degree of polarization between the lobes is shared by the jets. The only detectable polarized emission is in the south jet, where the **E** vectors are parallel to the jet axis near the core, and perpendicular further out. The degree of polarization $p_{4.9}$ is generally from 0.05 to 0.2 in the jet at this resolution, but reaches 0.5 ± 0.2 near the core on its south side. The jet cannot be much more strongly polarized at 15 GHz, as the polarized emission was barely detected anywhere along it at this frequency. Unfortunately, the low signal-to-noise of the polarized emission at 15 GHz prevents us from measuring the Faraday rotation near the jet at high resolution, and thus from establishing the **B** vector directions in the jet firmly. If the Faraday rotation in front of the jet at 4.9 GHz is small, the **B** vectors in the highly polarized region near the first knot are roughly perpendicular to the jet axis, while those in the less polarized region farther from the core are parallel to the axis. This field configuration would be unusual, but not unprecedented; the **B** parallel orientation usually dominates the interknot regions of the jets in powerful sources, but local perturbations have been detected at bright knots in other radio jets (Bridle 1986). The unusual configuration may, however, be a symptom of a large Faraday rotation at the center of 3C 288.

IV. DISCUSSION

a) The Large-Scale Structure

To estimate the equipartition magnetic field strengths B_{eq} in the lobes, we make the conventional assumptions that all relevant features are cylinders with depths equal to their Gaussian FWHM on the plane of the sky, that the radio spectra are power laws from 10 MHz to 100 GHz, that the filling factor of the emission is unity, and that equal energies reside in relativistic electrons and "ions." With these assumptions, B_{eq} ranges from $\sim 35h^{2/7}$ to $75h^{2/7}$ μG over the lobes, the lower values prevailing in the more diffuse emis-

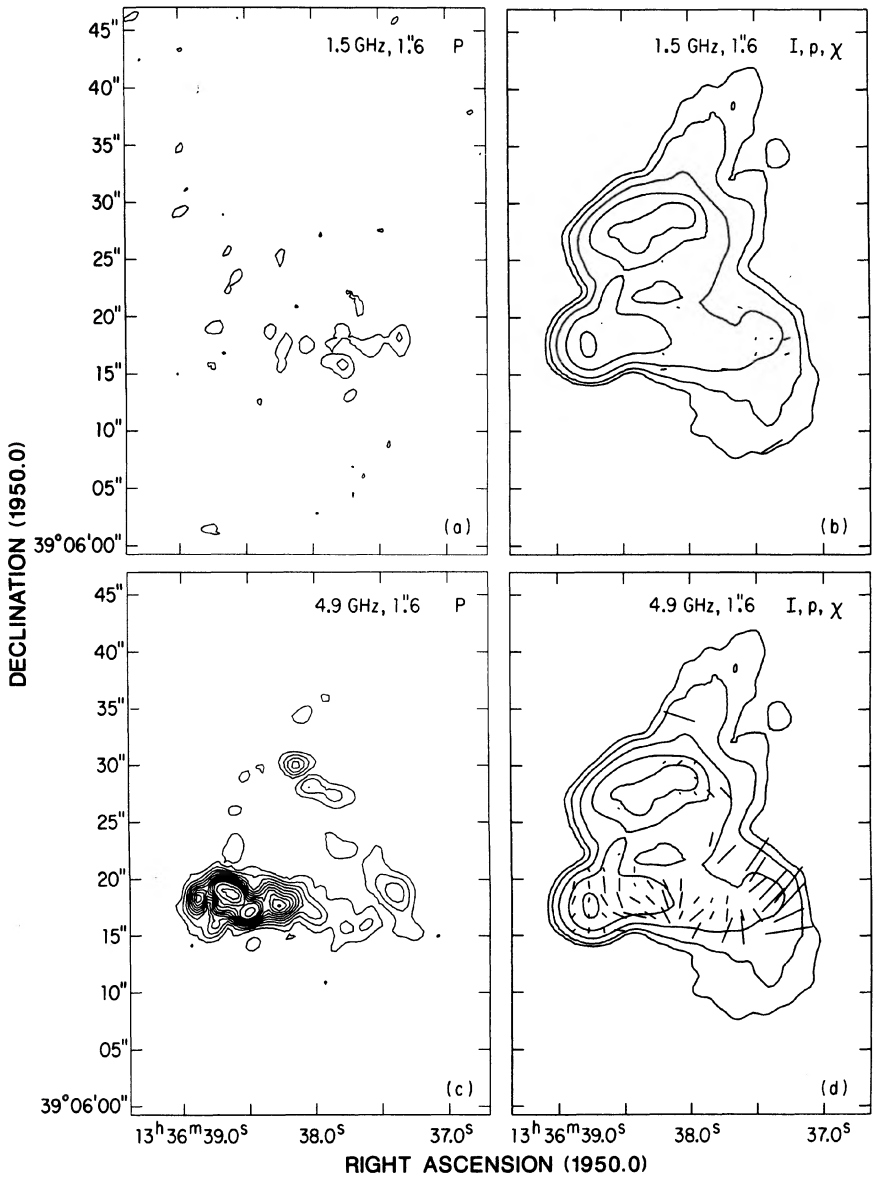

FIG. 6. Distributions of polarized intensity (left-hand panels—a and c) and of degree of polarization p and E vector position angles χ (right-hand panels—b and d) with 1".6 resolution at 1.5 and 4.9 GHz. Contours are drawn at 1 and 2 times 500 μJy per CLEAN beam area in panel a (1.5 GHz) and at 1, 2, 3, 4, 5, 6, 7, 8, 9, 10, 12, and 14 times 350 μJy per CLEAN beam in panel c (4.9 GHz). The contours in panels b and d are chosen to delineate the main features of the total-intensity distribution at 1.5 GHz shown in Fig. 1. The vectors in panels b and d have lengths proportional to $p_{1.5}$ and $p_{4.9}$, respectively (a vector of length 1" being equivalent to $p = 0.148$). Vectors are drawn at intervals of 1".45, wherever the polarized signal-to-noise ratio is $> 4{:}1$.

sion, and the higher values in the ridges and knots.

If we assume that the true magnetic field strengths are $\sim B_{\rm eq}$, we can obtain spectral-age benchmarks for any model that attributes the spectral gradients over 3C 288 to synchrotron losses without *in situ* particle reacceleration. We assume that the radiated spectrum of the particles at injection into the lobes is that of the jets, with $\alpha_{4.9}^{1.5} = 0.75$, and use the results of Myers and Spangler (1985, their Fig. 2) to convert the observed values of $\alpha_{4.9}^{1.5}$ to local spectral "ages."

Figure 8 plots these ages against distance measured westward from the easternmost peak along the ridge line of each lobe. In the south lobe, the ages increase almost monotonically from east to west, at a mean rate of $(0.15 \pm 0.02)h^{-3/7}$ Myr arcsec^{-1}. The general trend in the north lobe is similar, with a mean rate $(0.17 \pm 0.06)h^{-3/7}$ Myr arcsec^{-1}. Both Fig. 4 and Fig. 8 contain evidence for a more subtle variation of spectral age with position in the north lobe, however. Specifically, the spectral age of the bright western knot in the north lobe is $(0.47 \pm 0.05)h^{-3/7}$ Myr, within errors of the $(0.39 \pm 0.04)h^{-3/7}$ Myr age at the eastern peak. (Although the spectral index is greater at the western knot, the equipartition field strength is also higher.) Both the spectral index and the spectral age increase more rapidly northwest of this knot, the age gradient becoming $(0.51 \pm 0.02)h^{-3/7}$ Myr arcsec^{-1}.

The reciprocals of these age gradients translate to formal "velocities" of $(15\,000 \pm 2000)h^{-4/7}$ km s^{-1} for the south lobe, and of $(4400 \pm 200)h^{-4/7}$ km s^{-1} at the west end of the north lobe. These values greatly exceed the observed velocity dispersions of clusters of galaxies, and the observed peculiar velocities of brightest cluster members. The spectral gradients cannot therefore be solely due to aging of unreaccelerated electrons in equipartition magnetic fields left behind 3C 288 as it moves across the line of sight through an intracluster medium.

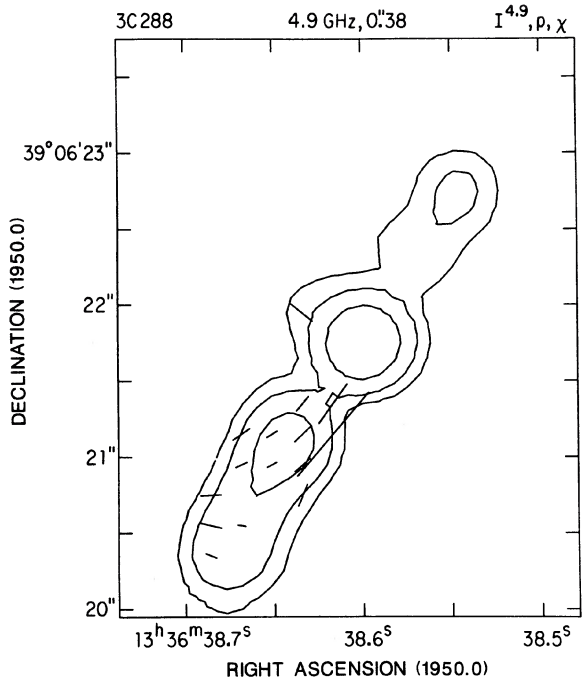

FIG. 7. Distribution of the degree of polarization $p_{4.9}$ and **E** vector position angle χ over the jet with 0."38 resolution at 4.9 GHz, superimposed on selected contours from Fig. 3(a). The vectors have lengths proportional to $p_{4.9}$ (a vector of length 1" being equivalent to $p_{4.9} = 1$). The vectors are drawn at intervals of 0."2 wherever the polarized signal-to-noise ratio is > 2:1.

This is a familiar result, even for fast-moving narrow-trail sources (e.g., IC 711—Wilson and Vallée 1977; 1605 + 35—Ekers *et al.* 1978; 3C 129—Downes 1980). It is often cited as evidence for particle reacceleration along such trails, or for magnetic fields being below their equipartition values (so that the synchrotron ages are underestimated). An alternative that may be more relevant in sources as powerful as 3C 288 is that there may be bulk flow velocities of order 10 000 km s^{-1} within the radio structure. Section IV*d* discusses this alternative in some detail.

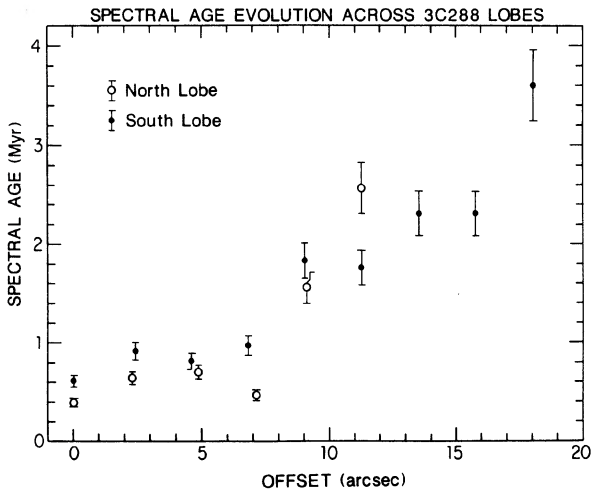

FIG. 8. Variation of the spectral age in megayears across the ridge lines of the north and south lobes at 1."6 resolution, plotted against the offset in arcseconds from the easternmost peak of the ridge.

To summarize, our observations confirm that 3C 288 has an edge-darkened outer structure in which the 1.5–4.9 GHz spectral indices increase toward the outer parts of the source. These properties of 3C 288 resemble those of class I (low-power) sources in the Fanaroff and Riley (1974) classification. We also find, however, that 3C 288 has features—the knot at the peak in the north lobe, and the ridge at the east end of the south lobe—that could be "incipient hotspots" characteristic of the more powerful Fanaroff–Riley class II sources. These features are near the projected axis of the radio jet and counterjet, have low spectral ages, and adjoin steep brightness gradients in the more extended emission. They also have the polarization structure (**E** vectors parallel to the steepest brightness gradients) that is normal near the hotspots of classical doubles. The large-scale structure can therefore be characterized as "transitional" between the two main Fanaroff–Riley classes.

b) The Jet and Counterjet

The principal knots in the jet and counterjet are not collinear with the core, but the deviations from collinearity are **S** symmetric about the core rather than **C** symmetric, unlike most radio trails whose jets have been clearly resolved. There could, of course, be **C** symmetry in the unseen (radial) direction, but the apparent geometry of the jet and counterjet contains nothing to encourage classifying 3C 288 as a radio-trail structure.

The jet is everywhere brighter than the counterjet at both 4.9 and 15 GHz. The peak of the counterjet occurs near its tip, 1."15 ($2.8h^{-1}$ kpc) from the core, opposite a plateau in the brightness of the main jet. The outermost peak of the main jet is 1."5 from the core, significantly further from the core than the outermost peak of the counterjet. In this sense, the scale of the main jet is 1.3 times that of the counterjet. Because of this geometrical asymmetry, the ratio between the 4.9 GHz brightnesses of points along the jet and counterjet that are *equidistant* from the core oscillates from 1.8:1 to > 30:1 with distance from the core. If we instead measure brightness ratios at 4.9 GHz between pairs of points whose distances from the core are in the 1.3:1 scale ratio, they range from 1.95:1 (at the two jet tips) to 6:1 (closer to the core).

The brightness ratios between the jet and counterjet are also frequency dependent, as can be inferred from their differing radio spectra. At 0."38 resolution, the 15 GHz brightness ratios between the main jet and the counterjet vary from 3:1 to > 8:1. There are few data on the spectra above 5 GHz for jets in other powerful sources, so we cannot judge how common this effect might be.

Bridle (1984, 1986) classified jet/counterjet systems as "one sided" if the brightness ratio is > 4:1 everywhere that the dynamic range of the data allow it to be measured, and "two sided" if the ratio is < 4:1 everywhere that the brighter jet can be detected. He characterized the jet and counterjet in 3C 288 as having transitional sidedness on this scheme, owing to the variation in their brightness ratio both with distance from the core and with observing frequency. In his sample of 136 sources with jets and known redshifts, the transition from mainly two sided to mainly one sided jets occurs near a 1.4 GHz total power of $P_{1.4} = 10^{25} h^{-2}$ W Hz^{-1} and a 5 GHz core power of $P_5 = 10^{23.5} h^{-2}$ W Hz^{-1}, with a dispersion of about a factor of 10 in each parameter. The core power of 3C 288,

$P_5 = 7.0h^{-2} \times 10^{23}$ W Hz^{-1}, is therefore "normal" for a source with transitional jet symmetries, although its total power ($P_{1.5} = 2.5h^{-2} \times 10^{26}$ W Hz^{-1}) is well above the typical transition regime. 3C 288 thus exemplifies the trend, noted by Bridle (1986), for core radio powers to predict jet symmetries better than total radio powers.

The physical origin of jet sidedness is controversial—e.g., Bridle and Perley (1984) and references therein. Our observations contain nothing that helps to resolve the controversy over whether jet sidedness on kiloparsec and larger scales reflects intrinsic asymmetries—e.g., "flip-flop" behavior (Rees 1976, 1981; Willis *et al.* 1978; Rudnick and Edgar 1984), side-to-side differences in the intrinsic synchrotron emissivities (van Groningen *et al.* 1980; Rees 1981), anisotropic pitch-angle distributions for the radiating particles (van Groningen *et al.* 1980)—or bulk relativistic effects (Scheuer and Readhead 1979; Blandford and Königl 1979). All the brightness and geometrical asymmetries in the jet/counterjet system cf 3C 288 could be attributed (in an entirely *ad hoc* way) to side-to-side differences, or temporal variations, in the energy output, relativistic electron content, or magnetic fields in the outflows from the central engine; or to asymmetries in the interactions between the jets and inhomogeneities in the ambient medium. We note, however, that all the asymmetries of the jet and counterjet are of the kind expected if 3C 288 has intrinsically symmetric, bipolar relativistic jets that have *restarted* after being inactive. Bridle *et al.* (1986) discussed such a model in detail for 3C 219, so we merely outline it here.

Jets that restart after a dormant phase must develop strong outward-moving shock structures at their tips as they re-establish their channel through the ambient medium. To first order, we can expect the flows to have characteristic velocities $v_j = \beta_j c$ near the core until they reach shocks with outward velocities $v_s = \beta_s c < v_j$. The brightness ratio between the preshock flows produced by Doppler favoritism will be

$$\left(\frac{1+\beta_j \sin \iota}{1-\beta_j \sin \iota}\right)^{2+\alpha},$$

where ι is the angle between $\mathbf{v}_j$ and the plane of the sky and α is the jet spectral index. The tips of the jet and counterjet will have apparent separations from the core whose ratio is

$$\left(\frac{1+\beta_s \sin \iota}{1-\beta_s \sin \iota}\right).$$

At the tips of the jets, deceleration of the flow reduces the brightness ratio at least to

$$\left(\frac{1+\beta_s \sin \iota}{1-\beta_s \sin \iota}\right)^{2+\alpha},$$

and perhaps further by disordering the velocities.

"Born-again" jets should thus exhibit the following general characteristics: (a) neither the jet nor the counterjet extends all the way to the lobes; (b) the tip of the counterjet appears to be closer to the core than the tip of the main jet; and (c) the brightness ratio between the tips of the jets is less than the ratio closer to the core. The jet and counterjet in 3C 288 match all three of these characteristics. The observed 1.3:1 ratio of their lengths requires $\beta_s \sin \iota = 0.13$. Solutions therefore exist for any $\iota > 7°.5$. For a source with $\iota = 30°$, its average value in a randomly oriented sample, a shock velocity v_s of $0.26c$ will account for the geometric asymmetry. The brightness ratio between the tip of the main jet and the tip of the counterjet should be $< (1.3)^{2.75}$:1, i.e., < 2.05:1 whatever the separate values of ι and β_s. The observed ratio is 1.95:1 at 4.9 GHz. The observed increase in the brightness ratio to 6:1 toward the core at 4.9 GHz would correspond to a preshock jet velocity v_j of $0.63c$ at $\iota = 30°$. The parameters are obviously far from definitive, as we have no independent measure of the inclination angle ι (and the velocity field in a born-again jet is likely to be more complex than this simple description assumes). They do, however, illustrate that only a mildly relativistic flow would be needed to account for the observed asymmetries, and that these asymmetries could be seen for a wide range of orientations of the jets relative to the observer.

The *sense* of the observed radio spectral-index difference between the jet and counterjet in 3C 288 also fits a relativistic-jet picture. If the intrinsic (rest-frame) radio spectrum steepens with increasing frequency equally in both jets (e.g., from synchrotron losses) the (redshifted) counterjet should have a steeper spectrum than the (blueshifted) main jet at high frequencies. The *magnitude* of the spectral-index difference, 0.6 ± 0.2, is surprising, however. For the parts of the jet and counterjet emission that arise from material traveling at the shock velocity v_s, the ratio between the intrinsic emission frequencies in the jet and counterjet is the ratio of their Doppler factors, i.e.,

$$\left(\frac{1+\beta_s \sin \iota}{1-\beta_s \sin \iota}\right).$$

This equals the ratio of the apparent separations of their tips from the core, which our data constrain to be 1.3:1, regardless of the separate values of β_s and ι. For parts of the jet and counterjet emission that arise from the preshock flow, the ratio of the Doppler factors is

$$\left(\frac{1+\beta_j \sin \iota}{1-\beta_j \sin \iota}\right),$$

which is constrained by the inner brightness ratio to be about 1.9:1. As the jet tips are not well resolved, the emission whose spectrum we have measured is probably a blend of these two cases, so the symmetric relativistic-jet picture asks that the intrinsic spectrum steepens by 0.6 ± 0.2 with only a 30%–90% increase in frequency. This is physically possible, but only if even the lower spectral index (0.72 ± 0.04) is increased significantly by synchrotron losses. The spectral curvature should continue below 4.9 GHz, and we should expect $\alpha_{4.9}^{1.5} \leqslant 0.5$, even if most of the jet and counterjet emission comes from the preshock region. This prediction is not supported by the integrated 1.5–4.9 GHz spectral index that we derived in Table III, or by preliminary reductions of a MERLIN 0.4 GHz image of 3C 288 at 1″ resolution (D. Stannard, private communication). We note, however, that the counterjet emission is so faint at 15 GHz that the nonlinear CLEAN deconvolution, and hence the model fed back to our self-calibration procedure, may have discriminated against it. This effect could exaggerate the apparent spectral-index asymmetry and thus imply a greater spectral curvature than is actually present. Both the spectral curvature and this possible observational bias can be explored using more sensitive high-resolution imaging of 3C 288, and we plan to acquire such data. Until this has been done, we conclude that the spectral asymmetry is qualitatively, but perhaps not quantitatively, of the kind expected in a symmetric relativistic-jet model.

Finally, the increase in depolarization toward the center

of the source in the south lobe, and the evidence for higher depolarization in the north lobe, are both consistent with a geometry in which a depolarizing medium surrounds the jets and lobes of 3C 288 symmetrically, and the brighter jet is on the side oriented toward us. This is the geometry required by a relativistic-jet model for the jet/counterjet asymmetries.

To summarize, 3C 288 is transitional in its observed jet properties, as well as in its lobe properties. Many attributes of the jets can readily be explained if their outflows have recently restarted with mildly relativistic bulk velocities, for a wide range of jet orientations. The jets do not exhibit the C symmetry characteristic of those in narrow radio "trails."

c) The Slingshot Model of 3C 288

Valtonen (1976) and Byrd and Valtonen (1980) modeled the brightness distribution of 3C 288 as an aggregate of plasma clouds created by two supermassive objects ejected simultaneously from the nucleus and repeatedly orbiting past it as the galaxy travels from west to east at ~ 175 km s^{-1}. They adopted a typical spectral age of 50 Myr at 1.4 GHz, much greater than the ages derived in Fig. 8. Our new images have several characteristics that force revision of their picture.

First, the source has features in locations that were not predicted by the model—the wings extending from the lobes, and the complex of emission in the north lobe that lies east of the core, i.e., ahead of the proposed path of the nucleus and of the orbiting objects. Second, the lobes and wings are smoother than predicted by the model, especially at the west end of the source. The western blobs of emission in the model would have to be moved from their original positions away from the suggested path of the galaxy, and significantly expanded, to represent the observed wings.

The slingshot model avoids the spectral age, or "velocity," problem by postulating that the magnetic field strength in the lobes is about ten times less than its equipartition value—the 50 Myr spectral age assumed by Byrd and Valtonen corresponds to a magnetic field strength of 6.3 μG, including the effective field equivalent to inverse Compton scattering on the microwave-background radiation, which at $z = 0.246$ is itself 4.9 μG. This assumption of a low magnetic field strength cannot be challenged observationally, but it increases the energy requirements and the inferred internal pressure by $\sim 30\times$ over the equipartition values. These difficulties have been overcome in a new model, wherein a realistic flow pattern of intergalactic gas past the radio galaxy has been included in the simulation. This work will be described elsewhere (Valtonen and Kotilainen 1988). We now consider an alternative in which the structure reflects flow patterns like those inferred for "classical double" sources similar to 3C 288 in total radio power.

d) The Lobes as Secondary (Redirected) Flows

Evidence is mounting that large-scale secondary flows can determine the shapes of the fainter parts of powerful radio galaxies. Significant secondary flows are expected in powerful sources if the two main "flavors" of observable radio jet (Bridle 1984, 1986) are related to the two principal hydrodynamic jet propagation regimes (Payne and Cohn 1985; Norman *et al.* 1985) such that powerful sources contain *light* hypersonic outflows in which $\rho_{\rm jet} \ll \rho_{\rm ext}$. Momentum balance requires that the termination regions of such outflows advance into the surrounding medium much more slowly than the jet speed. Shocks and vortical motions in the termination regions can then convert the jet outflows into large-scale backflows if the jets are axisymmetric, or into secondary outflows in directions misaligned with those of the jets if they are not (Norman *et al.* 1985, and references therein; Williams and Gull 1985; Williams 1985). Empirically, there are at least two ways in which such secondary flows may be deflected away from the major axis of the source, producing complex radio structures.

Leahy and Williams (1984, henceforth referred to as LW) and Alexander and Leahy (1987) have shown that several galaxies with radio powers similar to that of 3C 288 have steep-spectrum extensions of their *inner* lobes (or "bridges") at right angles to their major axes. Good examples are 3C 52 ($P_{1.4} = 1.8h^{-2}\times 10^{26}$ W Hz^{-1}), 3C 165 ($P_{1.4} = 2.7h^{-2}\times 10^{26}$ W Hz^{-1}), and 3C 300 ($P_{1.4} = 3.1h^{-2}\times 10^{26}$ W Hz^{-1}). LW suggest that these extensions trace backflows that have been deflected away from the source axis as they propagate toward their galaxies. Such deflections may result from an asymmetry of the galactic atmosphere with respect to the backflow direction, or from the backflow entering a cavity created by earlier activity on a different axis. The deflections described by LW occur around $25h^{-1}$ to $50h^{-1}$ kpc from the galactic nuclei, i.e., on scales similar to, or larger than, the projected radius of 3C 288. They occur in radio features whose equipartition field strengths are typically only 5–10 μG, rather less than those in the lobes of 3C 288.

A further example of misaligned secondary flow can be seen in the *outer* lobes of the radio galaxy 3C 171 (Heckman *et al.* 1984), whose radio luminosity ($P_{1.4} = 2.6h^{-2}\times 10^{26}$ W Hz^{-1}) and projected linear size ($83h^{-1}$ kpc) are almost identical to those of 3C 288. 3C 171 has several long radio plumes extending from its hotspots almost at right angles to the axis defined by its brightest features. Such misaligned plumes can be understood as secondary outflows that have been redirected by oblique shocks in light primary jets that are not axially symmetric (Williams and Gull 1985; Williams 1985). The right-angled deflections in 3C 171 also take place about $10h^{-1}$ kpc from the galactic nucleus. They involve features whose equipartition field strengths are about $20h^{2/7}$ μG, closer to the values inferred for the lobes of 3C 288.

Given the difficulties attending trail-based interpretations of 3C 288, it is appropriate to ask whether the wings revealed by our VLA data can be interpreted as deflected backflows or secondary outflows. The south lobe structure could result if the main jet has obliquely shocked several times near the edge of the source and so has been converted to a secondary flow that deflected away from the jet and from the galaxy, as in 3C 171. The apparent angle of deflection in 3C 288 is intermediate between those in 3C 171 and in the initial backflows in the sources discussed by LW (where it is 180°). The north lobe structure of 3C 288 could result if an unsteady counterjet terminated in two different places in the last ~ 3 Myr, producing two steep-spectrum secondary flows whose outer parts form the wings. The superposition of two such flows could also help to explain the lower polarization of the north lobe at 4.9 GHz.

We note, however, that 3C 288 differs from many of the sources studied by LW, and from 3C 171, in that it lacks *prominent* hotspots. Such hotspots are believed to mark the near-shock regions where the outflow is initially redirected. These regions could, however, be inconspicuous in a given radio image if the jets are unsteady in time or in direction,

because the radiative lifetimes of particles near the shocks can be less than those in the secondary flows. Possible examples of backflow without prominent hotspots from within the LW sample are the southwest lobe of 3C 319, the northwest lobe of 3C 300, and the west lobe of 3C 285. The lack of strong hotspots in 3C 288 need not therefore invalidate this picture.

A feature that 3C 288 shares with trail sources is that its steep-spectrum wings extend far beyond the brighter parts of its lobes. Can this also be explained within a picture based on the properties of higher-power sources? The greater extension of the wings could be an artifact of projection if the axis of the primary flow in 3C 288 is near the line of sight and therefore appears foreshortened. We think it more likely that the extension is real, however, as such phenomena are not peculiar to 3C 288. The plume running north from 3C 171's west lobe extends much further from the galaxy than the primary hotspot. The sample studied by LW also contains several sources whose inner wings reach as far as, or further, from the core than their hotspots. It is unlikely that all of these sources are oriented near the line of sight. Section IV*b* also showed that the modest asymmetries of the jets in 3C 288 can be accounted for by relativistic effects without requiring an orientation near the line of sight. There is therefore no strong reason to suppose that the brighter features of 3C 288 are significantly foreshortened by projection, and we will presume that they are not.

Elongated *outer* plumes such as that in the west lobe of 3C 171 can be attributed to continued outflow into an inhomogeneous background medium, but J. P. Leahy (private communication) has pointed out that elongated *inner* wings are more problematic. They are unlikely to be produced by unaided backflow because this would require the ends of the wings to propagate away from the galaxy faster than the ends of the main lobes, which seems dynamically implausible. They may, however, be generated when backflows deflect into cavities created by earlier activity (as suggested by LW to explain the X-shaped structure of 3C 315). Long wings on deflected backflows may therefore be a by-product of a background inhomogeneity created by earlier activity in the source itself. Either of these interpretations may apply to 3C 288.

Our images of 3C 288 show a structure that is too convoluted for a convincing analogy to be drawn with any one similarly powerful source, even admitting some projection effects. Any attempt to model its unusual structure in detail in terms of redirected outflows or backflows would involve many more disposable parameters than we have observational constraints, especially about the surrounding pressure distribution. We believe, however, that the structure of 3C 288 may be interpreted by analogy with large-scale redirections of secondary flows and backflows, as seen in other similarly powerful sources. This analogy seems more promising than the alternatives based on ram-pressure bending of the primary outflows, as seen in low-power radio trails.

e) Commentary

Section III reports several qualitatively new radio features of 3C 288, but these features do not show conclusively how the source relates to other classes of radio galaxy. Its edge-darkened morphology and spectral-index gradients are reminiscent of the narrow-trail sources, but there is no other evidence that 3C 288 belongs to this class. Its association with a galaxy that is putatively the brightest member of a cluster, its radio power, and the steep-spectrum wing emerging from the north lobe would all be exceptional properties for a radio trail.

We have also found, however, that the source lacks the most definitive characteristics of a "classical double," i.e., conspicuous compact hotspots and edge brightening of its lobes. Nevertheless, a coherent description of its structure can be assembled, as in Sec. IV*d*, if the jets are light, mildly relativistic and unsteady, and have produced oblique secondary flows or backflows that do not envelop them. The internal pressures of the putative secondary flows in 3C 288 would be more than ten times higher than those of the detected backflows documented by LW (unless the source is oriented close to the line of sight so that we have overestimated energy densities throughout it), but are not much greater than those in the plumes of 3C 171. The detailed asymmetries of the jet and counterjet, the absence of prominent hot spots, and the multiple steep-spectrum wings in the northern lobe might all be related to unsteadiness of the primary outflows.

Our data therefore suggest that 3C 288 may be a "distorted double with unsteady jets," but they do not demand it. The source appears to be a particularly complex example of the ill-defined transition between the wide-angle tails and other distorted double structures associated with dominant galaxies in clusters or groups. Unfortunately, this statement does not clarify the physics of its distortions, as the origin of the deflections in wide-angle tails is itself obscure (Burns 1986). They might be produced by density inhomogeneities in the ambient medium, by interactions between radio structures and large-scale flows in this medium, or through deviations of current-carrying jets by large-scale magnetic fields. Given the small projected linear size of 3C 288, the motion of its host galaxy may also not be negligible, if there is subclustering or if the cluster core is not completely virialized (cf. Valtonen and Byrd 1986; O'Dea *et al.* 1987; Fitchett and Webster 1987; Mellier *et al.* 1988). What further observations might clarify the nature of 3C 288?

The redshifts of other candidate members of the cluster should be determined, to test whether 3C 288 is indeed a cluster member and to estimate its peculiar radial velocity. The peculiar velocity is also more likely to be small if the host galaxy is a cD with an extensive luminous halo (e.g., Beers and Geller 1983; Merritt 1984); evidence for such a halo would therefore also be helpful. The small size, confused morphology, and polarization asymmetries of 3C 288 raise the possibility that it is interacting strongly with ambient gas. Its gross polarization properties resemble those of 3C 277.3, in which such an interaction has been documented by finding extranuclear optical narrow-line emission that is closely correlated with the radio structure (van Breugel *et al.* 1985). Section IV*d* noted similarities between 3C 288 and 3C 171, which also has an extensive optical emission-line system that is well correlated with the radio structure (Heckman *et al.* 1984). A sensitive search for extended optical line emission around 3C 288 may therefore be productive. Spectroscopy could also test whether 3C 288 is interacting with the second galaxy that is projected on its radio structure. Our depolarization data suggest that the northern lobe of 3C 288 is observed through a magnetoionic medium that is Faraday thick by 5 GHz, so sensitive polarimetry with 0".4 or better resolution above 5 GHz will be valuable. X-ray evidence for, or against, the existence of a cooling flow around 3C 288 would also be of interest.

Finally, 3C 288 should be compared with two other sources with similar radio powers that have structures more typical of low-power sources. 3C 218 = Hydra A ($z = 0.065$, $P_{1.4} = 2.1h^{-2} \times 10^{26}$ W Hz^{-1}—Ekers and Simkin 1983; Baum *et al.* 1988), has an edge-darkened, plume-like radio structure, and 3C 433 ($z = 0.1016$, $P_{1.4} = 1.4h^{-2} \times 10^{26}$ W Hz^{-1}—van Breugel *et al.* 1983; Baum *et al.* 1988), has an asymmetric X-shaped structure. Both are associated with the brightest members of poor clusters. 3C 218 has a secondary nucleus 10″ ($8.5h^{-1}$ kpc) from the primary, and complex internal kinematics. 3C 433 has two nuclei 8″ ($10h^{-1}$ kpc) apart in a common optical envelope on the edge of a cluster, and line-emitting line filaments extending about 7″ ($9h^{-1}$ kpc) from its active nucleus. Both 3C 218 and 3C 433 may recently have participated in mergers. Models for 3C 288 in which the central engine and the jet axis have been perturbed during a merger may be particularly appropriate if 3C 288 has optical characteristics similar to these galaxies.

We are grateful to the VLA scheduling committee for suggesting this collaboration and for assigning time to the observations. Patrick Leahy made valuable comments on a draft of this paper, and reminded us of several similarities between 3C 288 and 3C 171. We also thank the referee, Larry Rudnick, for his thoughtful comments and questions. A. H. B. particularly thanks Ron Ekers and Steve Gull for some stimulating discussions about "born-again" relativistic jets. G. G. B. acknowledges support by an NSF/EPSCOR grant during part of this project.

REFERENCES

Alexander, P., and Leahy, J. P. (1987). Mon. Not. R. Astron. Soc. **225**, 1.

Baars, J. W. M., Genzel, R., Pauliny-Toth, I. I. K., and Witzel, A. (1977). Astron. Astrophys. Suppl. **61**, 99.

Baum, S. A., Heckman, T., Bridle, A., van Breugel, W., and Miley, G. (1988). Astrophys. J. Suppl. **68**, 643.

Beers, T. C., and Geller, M. J. (1983). Astrophys. J. **274**, 491.

Begelman, M. C., Rees, M. J., and Blandford, R. D. (1979). Nature **279**, 770.

Blandford, R. D., and Königl, A. (1979). Astrophys. J. **232**, 34.

Bridle, A. H. (1984). Astron. J. **89**, 979.

Bridle, A. H. (1986). Can. J. Phys. **64**, 356.

Bridle, A. H., Davis, M. M., Fomalont, E. B., and Lequeux, J. (1972). Astron. J. **77**, 405.

Bridle, A. H., and Perley, R. A. (1984). Annu. Rev. Astron. Astrophys. **22**, 319.

Bridle, A. H., Perley, R. A., and Henriksen, R. N. (1986). Astron. J. **92**, 534.

Burns, J. O. (1986). Can. J. Phys. **64**, 373.

Byrd, G. G., and Valtonen, M. J. (1980). Publ. Astron. Soc. Pac. **92**, 262.

Clark, B. G. (1980). Astron. Astrophys. **89**, 377.

Conway, R. G., Birch, P., Davis, R. J., Jones, L. R., Kerr, A. J., and Stannard, D. (1983). Mon. Not. R. Astron. Soc. **202**, 813.

Downes, A. (1980). Mon. Not. R. Astron. Soc. **190**, 261.

Ekers, R. D., Fanti, R., Lari, C., and Ulrich, M.-H. (1978). Astron. Astrophys. **69**, 253.

Ekers, R. D., and Simkin, S. M. (1983). Astrophys. J. **265**, 85.

Fanaroff, B. L., and Riley, J. M. (1974). Mon. Not. R. Astron. Soc. **167**, 31P.

Fitchett, M., and Webster, R. (1987). Astrophys. J. **317**, 653.

Garrington, S. T., Leahy, J. P., Conway, R. G., and Laing, R. A. (1988). Nature **331**, 147.

Goodson, R. E., Palimaka, J. J., and Bridle, A. H. (1979). Astron. J. **84**, 1111.

Heckman, T. M., van Breugel, W. J. M., and Miley, G. K. (1984). Astrophys. J. **286**, 509.

Högbom, J. A. (1974). Astron. Astrophys. Suppl. **15**, 417.

Laing, R. A. (1988). Nature **331**, 149.

Laing, R. A., and Peacock, J. A. (1980). Mon. Not. R. Astron. Soc. **190**, 193.

Leahy, J. P., and Williams, A. G. (1984). Mon. Not. R. Astron. Soc. **210**, 929 (LW).

Mellier, Y., Mathez, G., Mazure, A., Chauvineau, B., and Proust, D. (1988). Astron. Astrophys. **199**, 67.

Merritt, D. (1984). Astrophys. J. **276**, 26.

Myers, S. T., and Spangler, S. R. (1985). Astrophys. J. **291**, 52.

Norman, M. L., Winkler, K.-H. A., and Smarr, L. L. (1985). In *Physics of Energy Transport in Extragalatic Radio Sources*, Proceedings of the 9th NRAO Workshop, edited by A. H. Bridle and J. A. Eilek (NRAO, Green Bank), p. 150.

O'Dea, C. P., and Owen, F. N. (1985). Astron. J. **90**, 954.

O'Dea, C. P., Sarazin, C. L., and Owen, F. N. (1987). Astrophys. J. **316**, 113.

Payne, D. G., and Cohn, H. (1985). Astrophys. J. **281**, 655.

Pooley, G. G., and Henbest, S. N. (1974). Mon. Not. R. Astron. Soc. **169**, 477 (PH).

Quintana, H., and Lawrie, D. G. (1982). Astron. J. **87**, 1.

Rees, M. J. (1976). In *The Physics of Nonthermal Radio Sources*, Proceedings of the NATO Advanced Study Institute, edited by G. Setti (Reidel, Dordrecht), p. 107.

Rees, M. J. (1981). In *Origin of Cosmic Rays*, IAU Symposium No. 94, edited by G. Setti, G. Spada, and A. W. Wolfendale (Reidel, Dordrecht), p. 139.

Rudnick, L. (1985). In *Physics of Energy Transport in Extragalactic Radio Sources*, Proceedings of the 9th NRAO Workshop, edited by A. H. Bridle and J. A. Eilek (NRAO, Green Bank), p. 35.

Rudnick, L., and Edgar, B. K. E. (1984). Astrophys. J. **279**, 74.

Scheuer, P. A. G., and Readhead, A. C. S. (1979). Nature **277**, 182.

Schwab, F. R. (1980). Proc. SPIE **231**, 18.

Smith, H. E., and Spinrad, H. (1980). Publ. Astron. Soc. Pac. **92**, 553.

Steer, D. E., Dewdney, P. E., and Ito, M. R. (1984). Astron. Astrophys. **137**, 159.

Strom, R. G., and Conway, R. G. (1983). Astron. Astrophys. Suppl. **61**, 547.

Valtonen, M. J. (1976). Astrophys. J. **209**, 35.

Valtonen, M. J., and Byrd, G. G. (1986). Astrophys. J. **303**, 523.

Valtonen, M. J., and Kotilainen, J. (1988). In preparation.

van Breugel, W. (1980). Ph.D. thesis, Leiden University.

van Breugel, W., Balick, B., Heckman, T., Miley, G., and Helfand, D. (1983). Astron. J. **88**, 40.

van Breugel, W., Miley, G., Heckman, T., Butcher, H., and Bridle, A. (1985). Astrophys. J. **290**, 496.

van Groningen, E., Miley, G. K., and Norman, C. A. (1980). Astron. Astrophys. **90**, L7.

Wardle, J. F. C., and Kronberg, P. P. (1974). Astrophys. J. **194**, 249.

Williams, A. G. (1985). Ph.D. thesis, Cambridge University.

Williams, A. G., and Gull, S. F. (1985). Nature **313**, 34.

Willis, A. G., Wilson, A. S., and Strom, R. G. (1978). Astron. Astrophys. **66**, L1.

Wilson, A. S., and Vallée, J. P. (1977). Astron. Astrophys. **58**, 79.

Wyndham, J. D. (1966). Astrophys. J. **144**, 459.